RESEARCH ARTICLE

A low-cost, activated carbon-coated, stainless-steel counter electrode for dye-sensitized solar cells

M.A.K.L. Dissanayake*, T.S.M. Liyanage, J.M.K.W. Kumari, D.M.U.P.Sumanasekera, T. Jaseetharan, W.I. Sandamali and G.K.R. Senadeera

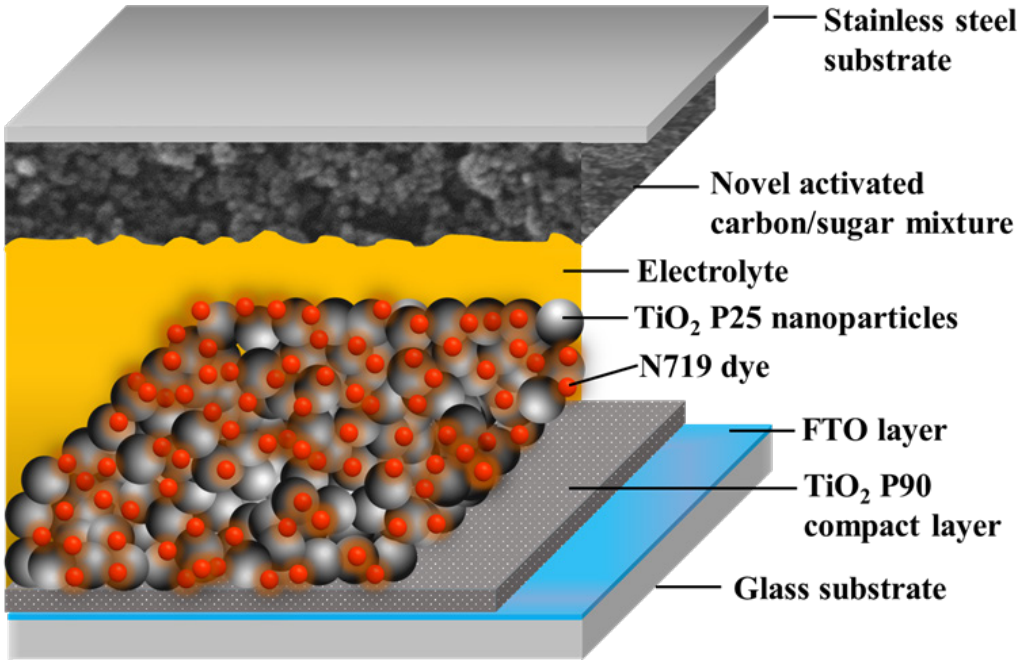

Highlights

- Activated carbon/stainless steel counter electrode for dye solar cells is developed.
- Dye solar cells with new electrode showed an energy conversion efficiency of 8.21%.
- The highest solar cell efficiency was 89% of that of Pt based solar cells.
- The new electrode showed high electrocatalytic activity with high specific surface area.
- Dye solar cells with activated carbon/FTO showed an efficiency of 7.50%.

Ceylon Journal of Science 53 (1) 2024: 109-118
DOI: http://doi.org/10.4038/cjs.v53i1.8237

RESEARCH ARTICLE

A low-cost, activated carbon-coated, stainless-steel counter electrode for dye-sensitized solar cells

M.A.K.L. Dissanayake[1,*], T.S.M. Liyanage[1,2,3], J.M.K.W. Kumari[1,4], D.M.U.P.Sumanasekera[1,2], T. Jaseetharan[1,5], W.I. Sandamali [1,6] and G.K.R. Senadeera[1,6]

[1]National Institute of Fundamental Studies, Hantana Road, Kandy, Sri Lanka
[2]Faculty of Engineering, University of Peradeniya, Peradeniya, Sri Lanka
[3]Department of Electrical and Electronics Engineering, Faculty of Engineering, University of Peradeniya, Peradeniya, Sri Lanka
[4]Postgraduate Institute of Science, University of Peradeniya, Peradeniya, Sri Lanka
[5]Department of Physical Sciences, South Eastern University of Sri Lanka, Sammanthurai, Sri Lanka
[6]Department of Physics, The Open University of Sri Lanka, Nawala, Nugegoda, Sri Lanka

Received: 21.09.2023; Accepted: 05.02.2024

Abstract: A low-cost, activated carbon (AC) and sugar-coated stainless-steel counter electrode for dye-sensitized solar cells was successfully fabricated and characterized. For performance comparison, a similar electrode was fabricated using a FTO glass as the substrate. The photovoltaic performance of dye-sensitized solar cells made with these two counter electrodes were compared with solar cells made with a Pt counter electrode. The optimized, activated carbon-coated, stainless-steel-based dye-sensitized solar cells showed an energy conversion efficiency of 8.21% while similarly optimized solar cells made with activated carbon-coated FTO counter electrode showed an efficiency of 7.50%. The efficiency of corresponding solar cells made with Pt counter electrode was 9.22%. The high solar cell efficiency of 89% of that of Pt based cells can be attributed to the high electro-catalytic activity and enhanced effective surface area of activated carbon/sugar composite and good electrical conductivity of stainless steel as demonstrated by electrochemical impedance spectroscopy, cyclic voltammetry, Tafel plot analysis and SEM imaging.

***Keywords*:** Dye-sensitized solar cells, stainless-steel, activated carbon, cyclic voltammetry, electrocatalytic activity.

INTRODUCTION

Dye-sensitized solar cells (DSSCs) are considered a low-cost alternative to the existing expensive silicon solar panels. While DSSCs are still in the research phase, considerable effort has been put into their efficiency enhancement and long-term stability (Grätzel et al., 2003; Wei et al., 2010). Recent advancements have resulted in DSSCs with efficiencies nearing 14% (Kakiage et al., 2015). Liquid electrolyte-based DSSCs typically consist of three main components: a photoanode, an electrolyte, and a counter electrode (CE). Each component plays a vital role in the overall cell mechanism. To photogenerate electrons, a light-absorbing dye is deposited on a mesoporous layer of a wide band gap semiconductor, usually TiO_2 or SnO_2 (Kumari et al., 2019; Kumari et al., 2016; Senadeera et al., 2018; Weerasinghe et al., 2021). The electrolyte provides the redox couple, which, as the name implies, acts as an electron junction for the cell (Dissanayake et al., 2020; Hodes et al., 2008; Kamat et al., 2010; Weerasinghe et al., *2021)*.

The most widely used counter electrode in DSSC is a thin layer of Pt coated on a fluorine-doped tin oxide glass (FTO) substrate (Yoon *et al.*, 2008). Both Pt and FTO are expensive materials and could limit the wide-scale applications of DSSCs (Syrrokostas et al., 2012). Therefore, the development of low-cost and chemically robust counter electrodes is an important and ongoing area of DSSC research that would enable these solar cells to compete with expensive silicon solar cells. The search for novel counter-electrode materials with high electro-catalytic activity and high electronic conductivity has identified some carbon-based materials such as graphite, reduced graphene oxide (RGO), activated carbon (AC), carbon nanotubes, etc. These materials also have additional advantages such as low cost, high surface area, high thermal stability, good corrosion resistance towards iodine, and high reactivity for triiodide reduction (Jayaweera et al., 2017; Nam et al., 2010; Suhas et al., 2007; Wang et al., 2012; Wibawa et al., 2020; Yun et al., 2014). Even though DSSCs fabricated with these counter electrodes have shown efficiencies comparable to or close to those with Pt counter electrodes, expensive FTO glass has been used as the substrate. These solar cells can be made even cheaper by replacing the FTO glass with alternative materials. Stainless steel (SS) is a low-cost and chemically stable material that can be used as a possible substrate for fabricating counter electrodes. However, not much research has been reported on developing stainless steel (SS) substrate-based counter electrodes for DSSCs (Calogera et al., 2010; Jun et al., 2007; Qin et al., 2010; Yu et al., 2013;). In this work, we report a highly efficient and low-cost counter electrode fabricated by coating activated carbon (AC) and sugar on a stainless steel (SS) substrate.

**Corresponding Author's Email: lakshman.di@nifs.ac.lk*
https://orcid.org/0000-0001-5488-9384

In selecting the materials, we have made use of the electrocatalytic properties of activated carbon, the adhesive properties of molten sugar, and the electrical conductivity of the stainless-steel substrate. This is the first report of the novel AC/sugar composite counter electrode. The best efficiency obtained for DSSC made with this novel counter electrode is about 89% of that of the Pt CE-based cells. A CE made using the same AC/sugar mixture on an FTO substrate, however, exhibited relatively lower solar cell efficiencies under identical conditions, highlighting the importance of stainless steel as a more suitable substrate material.

MATERIALS AND METHODS

FTO conducting glass substrates (8 /sq, Solaronix), Ruthenium N719 dye ($RuL_2(NCS)_2$:2TBA, Solaronix), titanium dioxide P-90 powder (Evonik), titanium dioxide P-25 powder (Degussa), polyethylene glycol (PEG 2000, Merck), triton X-100 (Merck), and hydrochloric acid (37%, Merck) were used as received without further purification to prepare the TiO2 photoanode. To prepare the redox electrolyte, iodine chips (I_2), acetonitrile (anhydrous), valeronitrile, guanidinium thiocyanate, and 4-tert-butylpyridine (TBP) (Sigma-Aldrich) were used. Ionic liquid PMII (1-propyl-3-methylimidazolium iodide) was purchased from Solaronix. Activated carbon (Sigma-Aldrich), white sugar (household), absolute ethanol (from VWR Chemicals), and SS or FTO were used to fabricate the novel CEs.

Preparation of the TiO_2 electrode

A TiO_2 P90 layer was deposited on a pre-cleaned FTO glass plate using the following method: 0.25 g of TiO_2 P90 powder was ground well with 1 ml of 0.1M HNO_3 for 15 min. This paste was then spin-coated on the FTO substrate for 60 s at 3000 rpm and sintered at 450 ^oC for 45 min. Subsequently, a TiO_2 P25 mesoporous layer was deposited on the TiO_2 P90 compact layer by the following method: 0.25 g of TiO_2 P25 powder was ground well with 1 ml of 0.1 M HNO_3, 1 drop of Triton X-100, and 0.05 g of PEG 2000 for 15 min. The P25 paste was deposited on the TiO_2 P90 compact layer by the doctor blading method and sintered at 450 ^oC for 45 min. These TiO_2 photoanodes were allowed to cool down to room temperature and were finally dipped in an ethanolic solution of Ru N719 dye for 15 hours for dye adsorption. (Kumari *et al.*, 2017).

Preparation of the liquid electrolyte

The liquid electrolyte was prepared by mixing 0.6 M 1-propyl-3-methylimidazolium iodide (PMII) ionic liquid, 0.03 M iodine (I_2), 0.1 M guanidinium thiocyanate, and 0.5 M 4-tert-butylpyridine (TBP) dissolved in acetonitrile: valeronitrile solution mixture in the volume ratio 85:15.

Fabrication of the Activated Carbon/Stainless Steel (AC/SS) and Activated Carbon/ FTO (AC/FTO) counter electrodes

Stainless steel (SS) sheet (1.50 mm thickness) was cut into 2 cm by 1 cm rectangular pieces. Each SS piece was smoothed using fine-grade sandpaper to get an even surface. Subsequently, the smoothed SS pieces were sonicated in soap water for 5 minutes to remove the dust and allowed to dry. 0.10 g of activated carbon (AC), 0.01 g of sugar, 2.0 ml of DI water, and 40 ml of ethanol were mixed and sonicated for 40 min. Sugar was used to improve the adhesion of AC to the SS or FTO substrate. While the solution was being sonicated, the SS piece was placed on a hot plate maintained at 100 ^oC. The mixture was sprayed on the hot SS surface several times to form uniform layers of AC. After spraying, the AC-coated SS CE was sintered at 150 ^oC for 1 hour for better adhesion and allowed to cool down to room temperature. These CEs were allowed to stabilize for 4-5 days to relieve the thermal stress before fabricating the solar cells. Similarly, AC was deposited on pre-cleaned FTO glass substrates following the same procedure as above to prepare AC/FTO counter electrodes to be used for performance comparison purposes.

Raman spectroscopy and XRD analysis of materials

The Raman spectra of the AC/sugar composite counter electrodes were obtained using a Renishaw basis instrument. The laser at 514 nm was used to take measurements. The crystalline structure of the proposed AC/Sugar composite powder was investigated with powder X-ray diffraction (PXRD) using the BrukerD8 advanced eco X-ray diffraction system with Cu Ka radiation (l = 1.54060 Å). XRD data were taken at 0.2 o step intervals in the 2-theta range of 10^o to 60^o.

SEM analysis

The surface morphology, cross-section, and structure of prepared AC/sugar composite CEs were studied using a scanning electron microscope (SEM-ZEISS).

DSSC Fabrication and Their Characterization

DSSCs were fabricated by sandwiching the liquid electrolyte between the TiO_2 photoanode and each of the newly designed counter electrodes: (a) AC/sugar on SS, (b) AC/sugar on FTO, and (c) Pt. The current density-voltage (*J-V*) characteristics of the solar cells were measured under the illumination of a 100 mW cm2 (AM 1.5) calibrated solar simulator (Oriel Newport LCS-100) coupled to a Metrohm Autolab Potentiostat/Galvanostat PGSTAT128N. A Xenon 100 W lamp was used with an AM 1.5 filter to obtain the simulated sunlight with the above intensity.

Electrochemical Impedance Spectroscopy (EIS) measurements were also performed on DSSCs using a Metrohm Autolab Potentiostat/GalvanostatPGSTAT128N with a FRA 32 M Frequency Response Analyzer (FRA) covering the frequency range between 1 MHz and 0.01 Hz under the illumination of 100 mW/cm^2 with the same solar simulator that was used for *J-V* measurements.

Cyclic voltammetry (CV) measurements

Cyclic voltammetry (CV) measurements were done to compare the electrochemical behavior of the three counter electrodes. The characteristic plots for each CE type were recorded using an iodide-based liquid electrolyte with a scan rate of 20 mV s^{-1} and a sweep potential of -0.4 V to 1.0 V. The supporting liquid electrolyte was made using 10 mM LiI, 0.1 M $LiClO_4$, and 1 mM I_2 dissolved in

acetonitrile. An Ag/AgCl/AgCl electrode was used as the reference electrode, and a Pt rod was used as the counter electrode. Newly prepared three CEs were used as the working electrode with an active cell area of 1.0 cm^2.

RESULTS AND DISCUSSION

XRD analysis and Raman spectroscopy analysis

Figure 1(a) shows the XRD pattern of the AC/sugar composite used to fabricate the counter electrodes. As shown in the figure, the strong diffraction peak at 2θ = 25° and the weak diffraction peak at 2θ = 45° characteristic of activated carbon can be seen, confirming the presence of activated carbon in crystalline form in the AC/Sugar composite of the counter electrode (Lazzarini et al., 2016; Wibawa et al., 2020). These peaks correspond to the diffraction of (002) and (100), respectively. The presence of very broad diffraction peaks and the absence of sharp peaks confirm the predominantly amorphous structure of the material. This lower degree of crystallinity shown by the broader XRD peaks confirms the mesoporous structure composed of AC crystallites in the AC/sugar composite. The AC grains of size about 40 nm seen in the SEM image (Fig. 2) appear to be composed of aggregates of activated carbon crystallites of size around 70–300 nm, forming the mesoporous structure and offering a large specific surface area available for catalytic redox reaction at the electrolyte/CE interface. Earlier studies have shown a specific area of 500–2000 m^2/g with substantial microporosity (Sudayanto et al., 2006; Suhas et al., 2007; Hu et al., 2001).

Raman spectroscopic analysis was carried out to characterize the novel AC/Sugar/SS CE. For activated carbon (AC), two main peaks in the Raman spectrum, consisting of a band consisting of the G band, arising from a first order in planer vibrational mode that originates from the doubly degenerate zone center E_{2g} phonon of sp^2 C, and a secondary D band arising from the transverse optical (TO) phonons near the K point in the Brillouin zone, could be seen. Figure 1(b) shows the Raman spectra of the AC/sugar composite. Prominent peaks can be seen at 1337 cm^{-1} and 1588 cm^{-1}, which correspond to the D and G bands, respectively (Lazzarini et al., 2016).

Morphology analysis

Figure 2(a) shows a SEM surface image of this electrode. The mesoporous nature of the CE surface can be verified by analyzing this figure. The higher electrocatalytic activity (ECA) of the AC/Sugar/SS CE compared to the platinum CE as described later in Section 2.5 can be attributed to the nanoporous structure with a much higher effective surface area of the counter electrode material in contact with the iodide/triiodide redox electrolyte. The grain sizes at several randomly selected places are marked in the image, and the average grain size was observed to be around 41 nm. The choice of activated carbon as the active counter electrode material can also be justified by its rough surface consisting of nano-sized grains, resulting in a greater number of active sites for iodide and tri-iodide reduction, and the unique network structure allowing rapid electron transfer and electrolyte diffusion.

A cross-sectional SEM image of an AC/Sugar/SS CE is shown in Figure 2(b). It can be seen that the thickness of the novel AC/sugar composite layer is in the micrometer range. The CE used for the SEM imaging shows an average thickness of 5.4 m. An increase in the effective surface area can be noticed by the nanoporous grain structure and the visibly folded surface nature of the composite electrode material. The higher electrocatalytic activity of the AC/Sugar/SS CE can be attributed to the increased effective surface area of the CE compared to the Pt and FTO-based CEs.

Photovoltaic performance of the DSSC

The photovoltaic performance of the DSSC fabricated using an AC/Sugar/SS counter electrode and an AC/Sugar/FTO glass counter electrode was determined. For comparison, DSSC made with sputtered Pt CE was also prepared and tested. To enhance the DSSC's performance, $TiCl_4$-treated photoanodes were used when fabricating these three different types of DSSCs. The $TiCl_4$ treatment allows the formation of small 3 nm-sized TiO_2 particles attached to the bigger ones, increasing the effective specific surface area available for dye loading, improving the interconnections between the larger TiO_2 particles, and creating additional pathways for the electrons to travel to

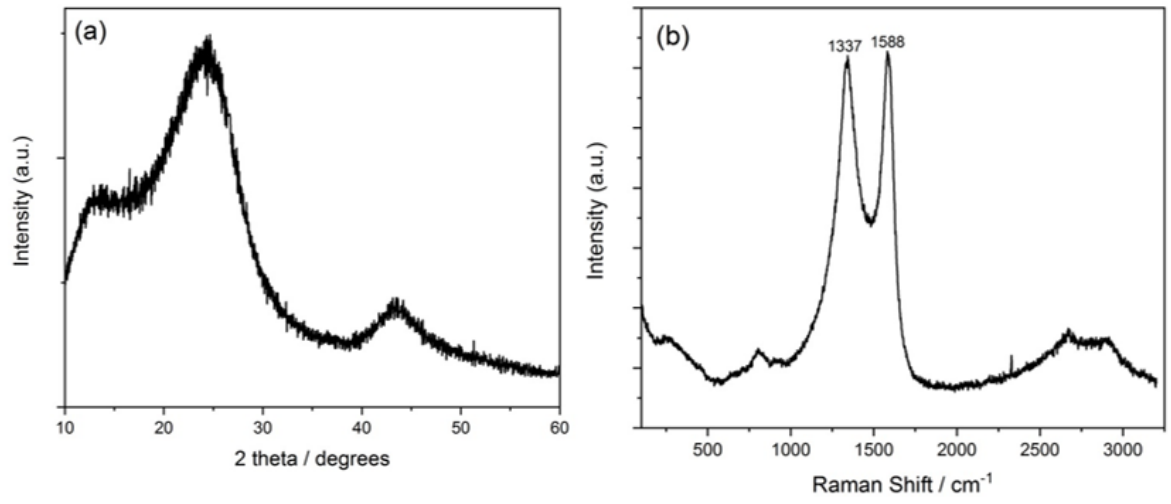

Figure 1: (a) XRD spectra of AC/Sugar composite and (b) Raman spectra of AC/Sugar composite.

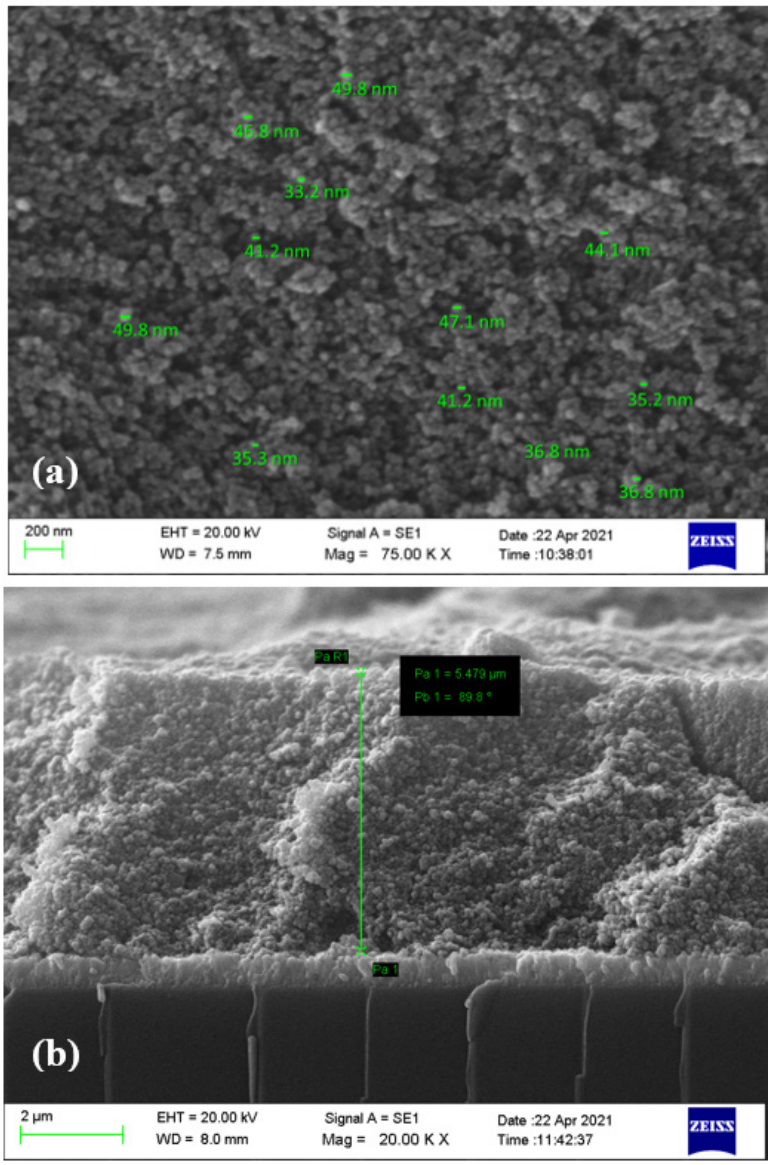

Figure 2: (a) Surface SEM image of the AC/sugar counter electrode with an average particle size is around 41 nm and, (b) cross-section view of the AC/sugar counter electrode with a thickness of 5.48 µm.

the conduction layer of the FTO plate, thereby increasing the photocurrent and the overall power conversion efficiency of the solar cell (Kumari et al., 2016). The current density-voltage (*J-V)* characteristics of the three different DSSCs made with the three types of counter electrodes and TiCl4-treated photoanodes are shown in Figure 3, and their photovoltaic parameters extracted from the figure are shown in Table 1.

When considering the above three solar cell structures made with the three counter electrodes, we observe that the DSSC made with the Pt CE has the highest efficiency of 9.22%. The DSSC made with the AC/Sugar deposited on SS CE shows an efficiency of 8.21%, while the DSSC made with the AC/Sugar deposited on FTO CE shows an efficiency of 7.50%. It is also observed that the DSSCs made with the Pt CE show the highest J_{SC} and the highest *Voc,* which contribute to the highest efficiency. The J_{sc} values of the DSSCs made with (a) AC/sugar on SS and (b) AC/sugar on FTO are comparable, but the V_{oc} and Fill Factor values are higher for the cells made with AC/sugar on SS CE, which gives the higher efficiency for the SS CE-based solar cell. It is interesting to note that the fill factor (FF) for the DSSCs made with AC/sugar on SS is higher than that of Pt CE-based DSSCs.

Electrochemical Impedance Spectroscopy (EIS) Analysis for DSSCs

Impedance and Bode phase data offer an insight into the working mechanism of a DSSC. Figure 4 shows the Nyquist plots of the DSSCs made with the three types of counter electrodes (a) Pt, (b) AC/sugar on SS, and (c) AC/sugar on FTO, respectively. The figure exhibits a large semicircle in the mid-frequency range for each device, which corresponds to the charge transfer resistance at the TiO_2 photoanode/electrolyte interface. The interface charge transfer resistance values were obtained by fitting the impedance parameters with the equivalent circuit model shown in the figures and using NOVA software.

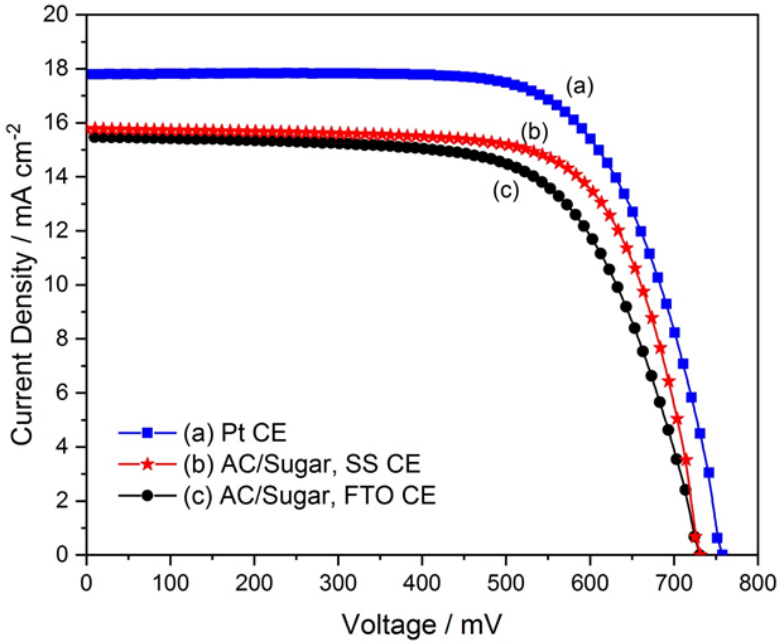

Figure 3: Current density-Voltage (*J-V*) characteristics of the DSSCs made with three counter electrodes, (a) Pt, (b) AC/sugar on SS and (c) AC/sugar on FTO.

Table 1: Photovoltaic parameters of DSSCs made with three counter electrodes (a) Pt, (b) AC/sugar on SS and (c) AC/sugar on FTO.

Counter electrode	J_{SC}/ mA cm^{-2}	V_{OC}/ mV	FF %	Efficiency %
(a) Pt	17.80 ± 0.20	762.60 ± 0.80	67.94 ± 0.40	9.22 ± 0.17
(b) AC/Sugar deposited on SS	15.80 ± 0.10	735.40 ± 0.90	70.70 ± 0.30	8.21 ± 0.10
(c) AC/Sugar deposited on FTO	15.50 ± 0.20	734.70 ± 0.70	65.85 ± 0.30	7.50 ± 0.13

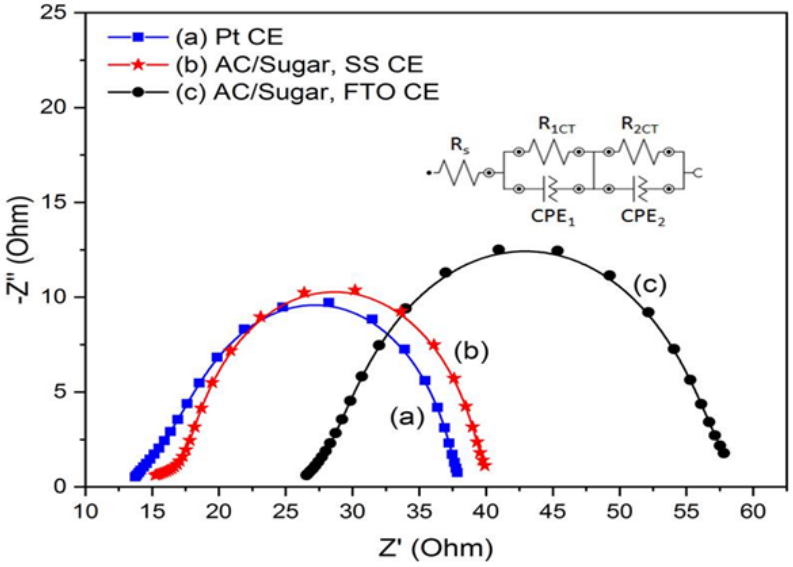

Figure 4: Nyquist plots of the DSSCs made with three counter electrodes (a) Pt , (b) AC/sugar on SS, and (c) AC/sugar on FTO.

The relevant resistance data extracted from the Nyquist plots is given below in Table 2. R_S, R_{1CT}, and R_{2CT} correspond, respectively, to the cell series resistance, resistance at the counter electrode/electrolyte interface, and resistance at the photoanode/electrolyte interface. However, $R1_{CT}$ is also related to the electrocatalytic activity of tri-iodide-to-iodine reduction taking place at the electrolyte/counter-electrode interface (Kumari et al., 2017; Wu et al., 2019; Yu et al., 2013). Usually, a lower R_{1CT} value is associated with higher electrocatalytic activity (ECA) (Kumar et al., 2017). It is interesting to see that the use of SS as the counter electrode substrate has significantly decreased the R_S value compared to the FTO glass substrate This can be attributed to the higher electrical conductivity of SS compared to FTO (Jun et al., 2007).

When the R_{1CT} values are considered, the DSSC made with AC/Sugar on SS CE has a lower resistance of 2.02 Ω, implying higher catalytic activity compared to the R_{1CT} value of 2.55 Ω obtained for the AC/Sugar on FTO. Hence, it is clear that SS offers a better substrate compared to FTO for AC to be used as counter electrodes in DSSCs. However, the lowest resistance values, R_s, *R1CT,* and *R2CT,* were obtained for the Pt CE-based DSSCs, and the next lower values were obtained with AC, Sugar, and SS CE-based DSSCs. The $R2_{CT}$ value is slightly higher in the AC/Sugar/SS CE system compared to the Pt CE system. The effect of the slightly higher $R2_{CT}$ of the AC/sugar/SS DSSC is manifested by a lower current density and lower efficiency compared to the Pt DSSC. The higher $R2_{CT}$ hinders the electron transfer mechanism at the electrolyte/photoanode interface, resulting in a lower overall efficiency (Dissanayake et al., 2017).

The AC/Sugar-SS electrode shows a smaller charge transfer resistance ($R2_{CT}$) at the electrolyte/electrode interface compared to the AC/Sugar-FTO electrode evidently due to the higher electronic conductivity of the SS substrate. This facilitates electrocatalytic activity towards the iodide/triiodide redox couple (Chang et al, 2013).

Cyclic Voltammetry (CV) analysis of counter electrodes

CV measurements were taken for all the counter electrodes with the iodide or tri-iodide redox species (the same electrolyte used in the DSSC) with respect to the Ag or AgCl reference electrode. The corresponding cyclic voltammograms (CV) are shown in Figure 5. In the CV graph, it can be observed that there are two peaks on each of the oxidation and reduction sides of the curves, which correspond to the following redox reactions (Chen *et al.*, 2016; Gong *et al.,* 2012).

$$I_3^- + 2e \rightleftharpoons 3I^- \quad (1)$$

$$3I_2 + 2e \rightleftharpoons 2I_3^- \quad (2)$$

The leftmost peak of the reduction side of the curve corresponds to reaction (1), while the rightmost peak corresponds to reaction (2). We are interested in reaction (1) since that is the rate-determining step for characterizing the electro-activity of the counter electrode since it catalyzes the reaction (1). Estimated peak current values corresponding to reduction (J_{Red1}), oxidation (J_{Ox1}), peak-to-peak voltage difference (E_p) for the peaks, and the diffusion coefficient (D_n) corresponding to reaction (1) are shown in Table 3.

From Table 3, it can be observed that the AC/Sugar-SS electrode exhibits both the lowest peak-to-peak separation

Table 2: EIS parameters of solar cells made with different counter electrodes.

Photoanode	Counter electrode	R_s (Ω)	R_{1CT} (Ω)	R_{2CT} (Ω)
TiO_2 treated with $TiCl_4$	(a) Pt	13.40	1.97	22.54
	(b) AC/Sugar-SS	15.07	2.02	22.99
	(c) AC/Sugar-FTO	26.42	2.55	29.06

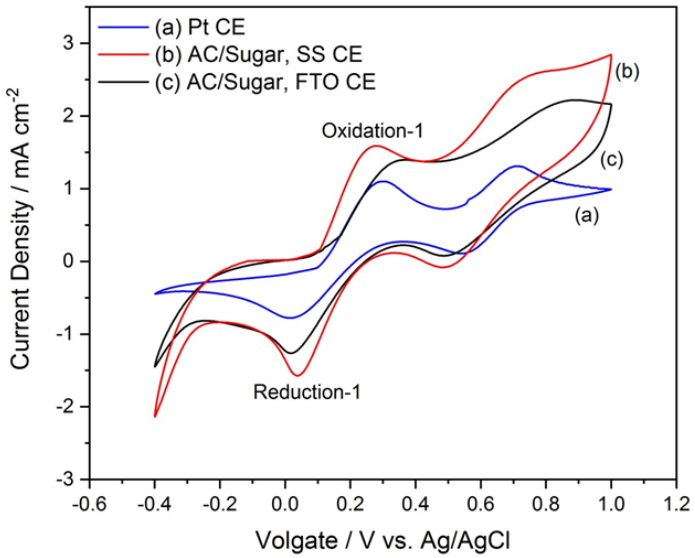

Figure 5: Cyclic voltammetry characteristics of the three counter electrodes taken at scan rate of 20 mVs^{-1}: (a) Pt, (b) AC/sugar-SS and (c) AC/sugar-FTO.

Table 3: Electrochemical parameters of the three counter electrodes estimated from the cyclic voltammetry measurements taken at scan rate of 20 mVs^{-1}: (a) Pt, (b) AC/sugar-SS and (c) AC/sugar- FTO.

Counter Electrode	J_{Ox1}/ mA cm^{-2}	J_{Red1}/ mA cm^{-2}	E_p / V	D_n ($\times 10^{-5}$)/ cm^2 s^{-1}
(a) Pt	1.07	-0.78	0.29	8.51
(b) AC/Sugar-SS	1.58	-1.56	0.23	12.04
(c) AC/Sugar-FTO	1.40	-1.26	0.34	10.82

voltage (E_p) and the highest peak currents (J_{Ox1} and J_{Red1}). Since the higher peak currents and lower peak-to-peak voltage difference suggest higher catalytic activity and better kinetic ability for reduction, we can conclude that AC/Sugar-SS CE has the highest catalytic activity out of all the 3 CEs (Fan *et al.,* 2015; Yang *et al.*, 2011).

CV measurements conducted on AC/Sugar-SS under different scan rates and the resulting cyclic voltammograms are shown in Figure 6(a). It is known that a freely diffusing reversible reaction follows the Randles–Sevcik equation given by,

$$J_{red1} = Kn^{1.5}ACD_n^{0.5}v^{0.5} \quad (3)$$

where K is the number of electrons in the reduction reaction, is the area of the electrode, is the concentration of the electrolyte, is the diffusion coefficient, and is the scan rate of the CV curve. Relatively larger D_n values are observed for both AC/Sugar-SS and AC/Sugar-FTO electrodes than the Pt electrode. According to the above equation, this can be associated with the thicker AC/sugar material on SS and the existence of a large number of bonding sites between AC and sugar, which can provide more active sites to reduce and accelerate charge transfer within the AC/sugar complex CE. It can be observed in Figure 6(a) that as the scan rate increases, the peak currents also increase, which is to be expected from the above equation. In addition, the positions of cathodic peaks are shifted towards negative potentials, while the peak positions of the anodic peaks are shifted to positive potentials with increasing scan rates. Also, according to Figure 6(b), there is a good linear relationship between the square root of scan rates and the oxidation and reduction peak current densities. This may indicate that the transport of I_3^- occurs by a diffusion-limited process and that the reaction is reversible (Subalakshmi *et al.*, 2019).

Tafel and EIS analysis of CEs

Tafel plots shown in Figure 7 were drawn for symmetric cells made from the three counter electrodes (a) Pt CE, (b) AC/Sugar-SS, and (c) AC/Sugar-FTO. The Tafel plots consist of three main phases. The end of each plot where the gradient of the plot is close to zero is the diffusion zone, which represents the process when diffusion rates become a limiting factor. Limiting diffusion current density J_{lim} calculated from this region gives an indication of the diffusion rate for each cell. The middle linear region is known as the Tafel region, where the logarithmic current density varies linearly with the overpotential. By extending the tangent of the Tafel zone and finding the intersection with the extended zero bias line, we can find the exchange current density (J_0) for each electrode. Points of very low potential are known as the polarization zone. The J_{lim} and J_o values calculated from Tafel curves are shown in Table 4.

According to Table 4, the CEs in decreasing order of J_{lim} are AC/Sugar-SS, Pt, and AC/Sugar- FTO. This implies that the cells with AC/Sugar-SS CE show better diffusion of the I^-/I_3^- redox species in the DSSCs followed by Pt and AC/Sugar-FTO. This can be confirmed by the CV analysis. The close agreement of J_{lim} values of Pt and AC/sugar/SS CEs verifies close diffusion coefficient values. The exchange current density is inversely proportional to the charge transfer resistance and is governed by the equation 4,

$$J_0 = \frac{RT}{nFR_{ct}} \quad (4)$$

where R,T, n, and F are the gas constant, absolute temperature, the number of electrons involved in the redox reaction, and the Faraday constant, respectively. Thus, a higher value of J_0 implies a lower charge transfer resistance (R_{ct}). R_{ct} is determined by factors such as the ECA, surface

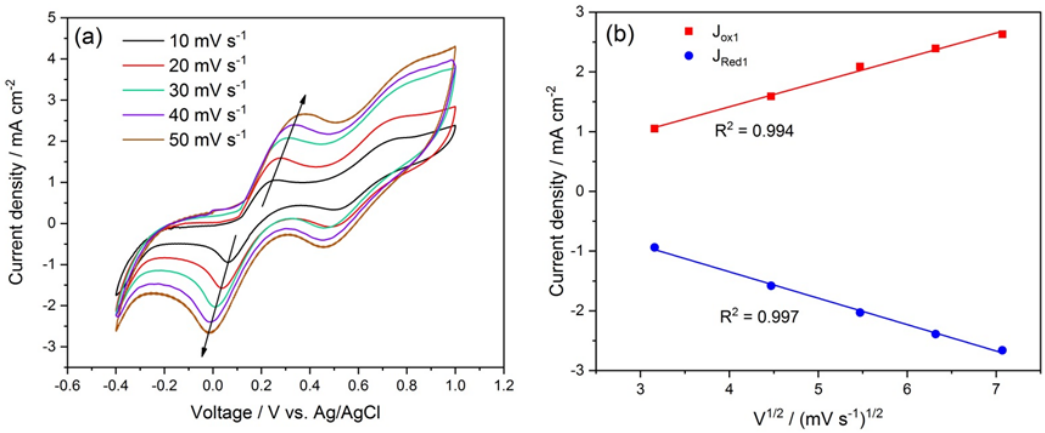

Figure 6: Cyclic voltammetry graphs for AC/Sugar/SS CE at different scan rates.

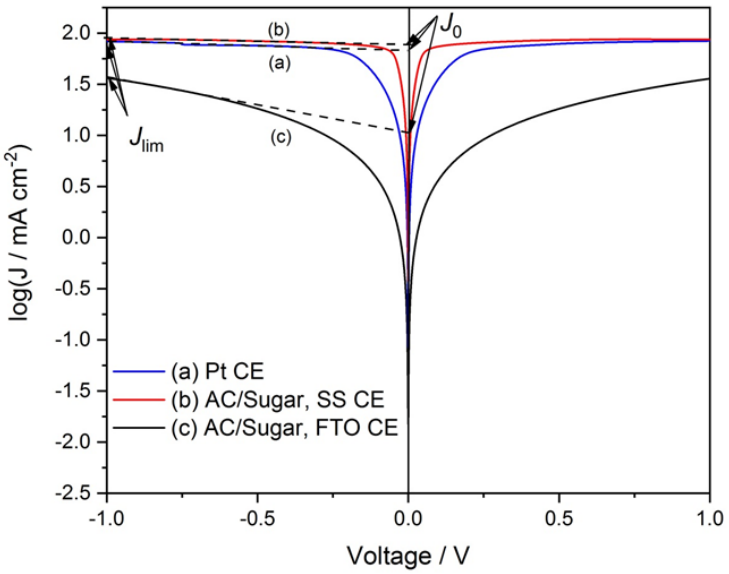

Figure 7: Tafel plots drawn for symmetric cells made from the three counter electrodes (a) Pt, (b) AC/Sugar on SS and AC/Sugar on FTO.

Table 4: J_{lim} and J_0 values obtained from the Tafel plots, R_s and R_{ct} values obtained from the EIS plots.

Counter electrode	J_o / mA cm^{-2}	J_{lim} / mA cm^{-2}	R_s / Ω cm^{-2}	R_{ct} / Ω cm^{-2}
(a) Pt	1.84	1.92	6.80	1.40
(b) AC/Sugar-SS	1.88	1.94	6.56	1.10
(v) AC/Sugar-FTO	1.03	1.56	12.42	15.40

roughness, material qualities, and thickness of the CE material. Figure 2 shows the AC/Sugar composite layer thickness on the micrometer scale. However, it has been suggested that the thickness of the Pt layer is on the nanometer scale (Fang et al., 2004). It can be seen that the J_0 values trend in the AC/Sugar-SS > Pt > AC/Sugar-FTO Conversely, this implies that R_{ct} is lowest in the AC/Sugar-SS CE and highest in the AC/Sugar-FTO CE. This confirms the highest ECA of AC/Sugar-SS from CV analysis.

To understand the improvement in ECA, EIS experiments were carried out with symmetrical cells fabricated with two identical CEs. The EIS spectra of symmetrical cells based on three types of CEs are shown in Figure 8. The series resistance (R_s) is mainly composed of the bulk resistance of CE material, and the radius of the large semicircle is attributed to the charge transfer resistance (Rct) at the CE/electrolyte interface. The values of R_s and *Rct* were extracted by fitting the EIS graph with the equivalent circuit indicated in the inset of Figure 8, and the values are tabulated in Table 4. The smallest R_{ct} of AC/Sugar, SS composite CE suggests a rapid conversion reaction from to, therefore resulting in an enhanced FF comparison with the other two types of CE-based devices (Yang et al., 2015). Also, the R_{ct} varies inversely with the electrocatalytic activity for the reduction reaction; such a decrease in R_{ct} demonstrates that the AC/Sugar/SS complex CE has the highest electrocatalytic activity. Therefore, the conclusions for the ECA and diffusion derived from the CV, EIS, and Tafel data are consistent, and it can be confirmed that the AC/Sugar composite in the SS substrate is a promising candidate to replace Pt as a CE in DSSCs.

CONCLUSION

The photovoltaic performance of DSSCs fabricated with three different counter electrodes, (a) Pt, (b) activated charcoal and sugar on stainless steel (SS), and (c) activated charcoal and sugar on FTO glass, has been compared. DSSCs fabricated with the novel counter electrode AC/sugar on SS exhibited an efficiency of 8.21% compared to 9.22% for Pt and 7.50% for AC/sugar on FTO.

The high solar cell efficiency of the cells made with activated carbon-coated stainless steel electrodes can be attributed to the high electro-catalytic activity and enhanced effective surface area of activated charcoal/sugar composite and the good electrical conductivity of stainless steel, as demonstrated by electrochemical impedance spectroscopy, cyclic voltammetry, Tafel plot analysis, and SEM imaging. The AC/Sugar coated SS counter electrode with a DSSC efficiency of 89% of that of Pt is a highly promising and much less expensive candidate to replace Pt as the counter electrode in DSSCs.

ACKNOWLEDGEMENT

Authors gratefully acknowledge the National Science Foundation of Sri Lanka for providing research support under the Sri Lanka-Pakistan collaborative grant NSF-PSF/ICRP/2017/EA&ICT/04.

DECLARATION OF CONFLICT OF INTEREST

The authors declare no conflict of interest.

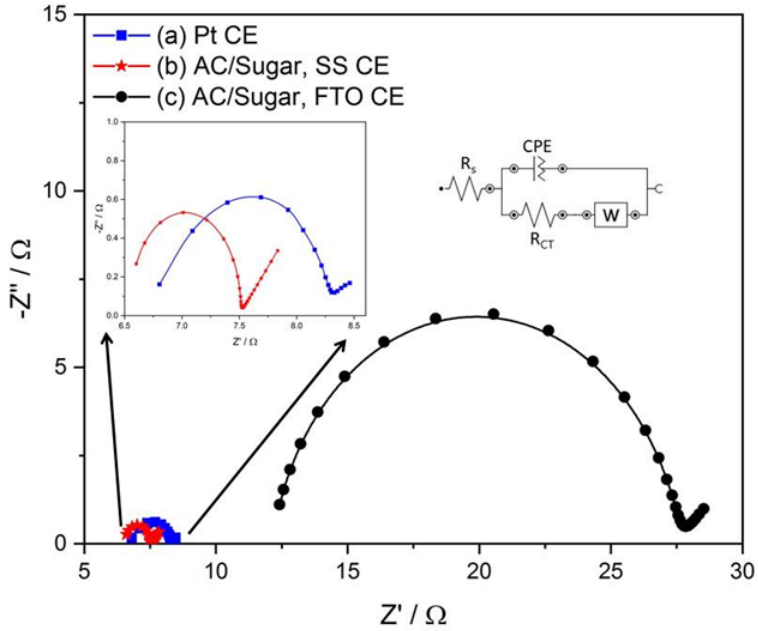

Figure 8: Electrochemical Impedance Spectra (EIS) of symmetric cells made from the three counter electrodes, (a) Pt , (b) AC/Sugar-SS, and (c) AC/Sugar-FTO.

REFERENCES

Calogero, G., Bonaccorso, F., Maragò, O. M., Gucciardi, P. G., & Di Marco, G. (2010). Single-wall carbon nanotubes deposited on stainless steel sheet substrates as novel counter electrodes for ruthenium polypyridine-based dye-sensitized solar cells. *Dalton Transactions* **39**(11): 2903. DOI: 10.1039/b922188h

Chang, L. H., Hsieh, C. K., Hsiao, M. C., Chiang, J. C., Liu, P. I., Ho, K. K., ... Tsai, C. H. (2013). A graphene-multi-walled carbon nanotube hybrid supported on fluorinated tin oxide as a counter electrode of dye-sensitized solar cells.
Journal of Power Sources **222**: 518–525. DOI: 10.1016/j.jpowsour.2012.08.036

Chen, M., & Shao, L. L. (2016). Review on the recent progress of carbon counter electrodes for dye-sensitized solar cells. *Chemical Engineering Journal* **304**: 629–645. DOI: 10.1016/j.cej.2016.07.129

Dissanayake, M. A. K. L., Kumari, J. M. K. W., Senadeera, G. K. R., Jaseetharan, T., Mellander, B.-E., Albinsson, I., & Furlani, M. (2020). Polyaniline (PANI) mediated cation trapping effect on ionic conductivity enhancement in poly(ethylene oxide) based solid polymer electrolytes with application in solid state dye sensitized solar cells. *Reactive and Functional Polymers* **155**: 104683. DOI:org/10.1016/j.reactfunctpolym.2020.104683

Dissanayake, M. A. K. L., Kumari, J. M. K. W., Senadeera, G. K. R., Thotawatthage, C. A., Mellander, B.E., & Albinsson, I. (2017). A novel multilayered photoelectrode with nitrogen-doped TiO2 for efficiency enhancement in dye-sensitized solar cells. *Journal of Photochemistry and Photobiology A: Chemistry* **349**: 63-72. DOI:org/10.1016/j.jphotochem.2017.08.067

Fan, M. S., Chen, J. H., Li, C. T., Cheng, K. W., & Ho, K. C. (2015). Copper zinc tin sulfide as a catalytic material for counter electrodes in dye-sensitized solar cells. *Journal of Materials Chemistry A* **3**(2): 562–569. DOI: 10.1039/c4ta04533j

Gong, F., Li, Z., Wang, H., & Wang, Z. S. (2012). Enhanced electrocatalytic performance of graphene via incorporation of SiO2 nanoparticles for dye-sensitized solar cells. *Journal of Materials Chemistry* **22**(33): 17321. DOI: 10.1039/c2jm33158b

Grätzel, M. (2003). Dye-sensitized solar cells. *Journal of Photochemistry and Photobiology C: Photochemistry Reviews* **4**(2): 145–153. DOI: 10.1016/S1389-5567(03)00026-1

Hodes, G. (2008). Comparison of Dye- and Semiconductor-Sensitized Porous Nanocrystalline Liquid Junction Solar Cells. *The Journal of Physical Chemistry* C **112**(46): 17778–17787. DOI: 10.1021/jp804360j

Hu, Z., & Srinivasan, M. (2001). Mesoporous high-surface-area activated carbon. *Microporous and Mesoporous Materials* **43**(3): 267–275. DOI: 10.1016/S1387-1811(01)00365-0

Jayaweera, E. N., Kumara, G. R. A., Pitawala, H. M. G. T. A., Rajapakse, R. M. G., Gunawardhana, N., Bandara, H. M. N., ... Yoshimura, M. (2017). Vein graphite-based counter electrodes for dye-sensitized solar cells. *Journal of Photochemistry and Photobiology A: Chemistry* **344**: 78-83. DOI: 10.1016/j.jphotochem.2017.06.031

Jun, Y., Kim, J., & Kang, M. G. (2007). A study of stainless steel-based dye-sensitized solar cells and modules. *Solar Energy Materials and Solar Cells* **91**(9): 779–784. DOI: 10.1016/j.solmat.2006.12.011

Kakiage, K., Aoyama, Y., Yano, T., Oya, K., Fujisawa, J., & Hanaya, M. (2015). Highly efficient dye-sensitized solar cells with collaborative sensitization by silyl-anchor and carboxy-anchor dyes. *Chemical Communications* **51**(88): 15894–15897. DOI: 10.1039/C5CC06632K

Kamat, P. V., Tvrdy, K., Baker, D. R., & Radich, J. G. (2010). Beyond Photovoltaics: Semiconductor Nanoarchitectures for Liquid-Junction Solar Cells.

Chemical Reviews **110**(11): 6664–6688. DOI: 10.1021/cr100243k

Kumar, R., Nemala, S. S., Mallick, S., & Bhargava, P. (2017). Synthesis and characterization of carbon-based counter electrode for dye-sensitized solar cells (DSSCs) using sugar-free as a carbon material. *Solar Energy* **144**: 215–220. DOI: 10.1039/c9na00206e

Kumari, J. M. K. W. K., Sanjeewadharshini, N., Dissanayake, M. A. K. L., Senadeera, G. K. R., & Thotawatthage, C. A. (2016). The effect of TiO2 photoanode film thickness on photovoltaic properties of dye-sensitized solar cells. *Ceylon Journal of Science* **45**(1): 33-41. DOI:10.4038/cjs.v45i1.7362

Kumari, J. M. K. W., Senadeera, G. K. R., Dissanayake, M. A. K. L., & Thotawatthage, C. A. (2017). Dependence of photovoltaic parameters on the size of cations adsorbed by TiO2 photoanode in dye-sensitized solar cells. *Ionics* **23**: 2895-2900. DOI: 10.1007/s11581-017-2047-4

Kumari, M. G. C. M., Perera, C. S., Dassanayake, B. S., Dissanayake, M. A. K. L., & Senadeera, G. K. R. (2019). Highly efficient plasmonic dye-sensitized solar cells with silver nanowires and TiO2 nanofibers incorporated multi-layered photoanode. *Electrochimica Acta* **298**: 330–338. DOI: 10.1016/j.electacta.2018.11.157

Lazzarini, A., Piovano, A., Pellegrini, R., Agostini, G., Rudić, S., Lamberti, C., & Groppo, E. (2016). Graphitization of Activated Carbons: A Molecular-level Investigation by INS, DRIFT, XRD and Raman Techniques. *Physics Procedia* **85:** 20–26. DOI: 10.1016/j.phpro.2016.11.002

Nam, J. G., Park, Y. J., Kim, B. S., & Lee, J. S. (2010). Enhancement of the efficiency of dye-sensitized solar cell by utilizing carbon nanotube counter electrodes. *Scripta Materialia* **62**(3): 148–150. DOI: 10.1016/j.scriptamat.2009.11.010

Qin, Q., Tao, J., & Yang, Y. (2010). Preparation and characterization of polyaniline film on stainless steel by electrochemical polymerization as a counter electrode of DSSC. *Synthetic Metals* **160**(11–12): 1167–1172. DOI: 10.1016/j.synthmet.2010.03.012

Senadeera, G. K. R., Weerasinghe, A. M. J. S., Dissanayake, M. A. K. L., & Thotawatthage, C. A. (2018). A five-fold efficiency enhancement in dye-sensitized solar cells fabricated with AlCl3 treated, SnO2 nanoparticle/nanofiber/nanoparticle triple layered photoanode. *Journal of Applied Electrochemistry* **48**: 1255-1264. DOI: 10.1007/s10800-018-1177-7

Subalakshmi, K., Kumar, K. A., Paul, O. P., Saraswathy, S., Pandurangan, A., & Senthilselvan, J. (2019). Platinum-free metal sulfide counter electrodes for DSSC applications: Structural, electrochemical and power conversion efficiency analyses. *Solar Energy* **193**: 507–518. DOI: 10.1016/j.solener.2019.10.070

Sudaryanto, Y., Hartono, S., Irawaty, W., Hindarso, H., & Ismadji, S. (2006). High surface area activated carbon prepared from cassava peel by chemical activation. *Bioresource Technology* **97**(5): 734–739. DOI: 10.1016/j.biortech.2005.04.008

Suhas, Carrott, P., & Ribeiro Carrott, M. (2007). Lignin – from natural adsorbent to activated carbon: A review. *Bioresource Technology* **98**(12): 2301–2312. DOI: 10.1016/j.biortech.2006.08.008

Wang, H., & Hu, Y. H. (2012). Graphene as a counter electrode material for dye-sensitized solar cells. *Energy & Environmental Science* **5**(8): 8182. DOI: 10.1039/c2ee22025e

Weerasinghe, A. M. J. S., Dissanayake, M. A. K. L., Senadeera, G. K. R., Senaviratne, V. A., Thotawatthage, C. A., & Kumari, J. M. K. W. (2017). Application of electrospun cellulose acetate nanofiber membrane-based quasi-solid-state electrolyte for dye-sensitized solar cells. *Ceylon Journal of Science* **46**(2): 93-98. DOI: 10.4038/cjs.v46i2.7433

Weerasinghe Janith, Suvanker Sen, S., Kumari, J. M. K. W., Dissanayake, M. A. K. L., Senadeera, G. K. R., Thotawatthage, C. A., & Ostrikov, K. (2021). Efficiency enhancement of low-cost metal free dye sensitized solar cells via non-thermal atmospheric pressure plasma surface treatment. *Solar Energy* **215**: 367-374. DOI: 10.1016/j.solener.2020.12.044

Wei, D. (2010). Dye-Sensitized Solar Cells. *International Journal of Molecular Sciences* **11**(3): 1103–1113. DOI: 10.3390/ijms11031103

Wibawa, P. J., Nur, M., Asy'ari, M., & Nur, H. (2020). SEM, XRD and FTIR analyses of both ultrasonic and heat generated activated carbon black microstructures. *Heliyon* **6**(3): e03546. DOI: 10.1016/j.heliyon.2020.e03546

Wu, K., Liu, Z., Wu, M., Ruan, B., Wu, R., Zhou, H., & Wu, M. (2019). Economically viable V2O3@activated carbon composite materials as counter electrodes for dye-sensitized solar cells by single step reduction. *Journal of Electroanalytical Chemistry* **835**: 150–155. DOI: org/10.1016/j.jelechem.2019.01.034

Yang, C. C., Zhang, H. Q., & Zheng, Y. R. (2011). DSSC with a novel Pt counter electrodes using pulsed electroplating techniques. *Current Applied Physics* **11**(1), S147–S153. DOI: 10.1016/j.cap.2010.07.040

Yoon, C. H., Vittal, R., Lee, J., Chae, W.-S., & Kim, K.-J. (2008). Enhanced performance of a dye-sensitized solar cell with an electrodeposited-platinum counter electrode. *Electrochimica Acta* **53**(6): 2890–2896. DOI: org/10.1016/j.electacta.2007.10.074

Yun, S., Hagfeldt, A., & Ma, T. (2014). Pt-Free Counter Electrode for Dye-Sensitized Solar Cells with High Efficiency. *Advanced Materials* **26**(36): 6210–6237. DOI: 10.1002/adma.201401746

Yu, K., Wen, Z., Pu, H., Lu, G., Bo, Z., Kim, H., ... Chen, J. (2013). Hierarchical vertically oriented graphene as a catalytic counter electrode in dye-sensitized solar cells. *Journal of Materials Chemistry A* **1**(2): 188–193. DOI: 10.1039/C2TA00156